Conformational Properties of Nickel(II) Octaethylporphyrin in Solution. 1. Resonance Excitation Profiles and Temperature Dependence of Structure-Sensitive Raman Lines

ARTICLE *in* THE JOURNAL OF PHYSICAL CHEMISTRY · AUGUST 1996

Impact Factor: 2.78 · DOI: 10.1021/jp9533032 · Source: OAI

Conformational Properties of Nickel(II) Octaethylporphyrin in Solution. 1. Resonance Excitation Profiles and Temperature Dependence of Structure-Sensitive Raman Lines

Walter Jentzen,*,†,‡ Esko Unger,† Gerasimos Karvounis,† John A. Shelnutt,‡,§ Wolfgang Dreybrodt,† and Reinhard Schweitzer-Stenner*,†

FB1-Institut für Experimentelle Physik, Universität Bremen, P.O. Box 330440, 28334 Bremen, Germany, Fuel Science Department, Sandia National Laboratories, Albuquerque, New Mexico 87185-0710, and Department of Chemistry, University of New Mexico, Albuquerque, New Mexico 87131

Received: November 7, 1995; In Final Form: March 26, 1996[⊗]

We have measured polarized resonance Raman spectra of nickel(II) octaethylporphyrin in CS_2 and CH_2Cl_2 solution at different excitation wavelengths (430−580 nm) and temperatures (190−310 K). The analysis of the spectra revealed that the structure-sensitive Raman lines ν_{19} and ν_{10} can be decomposed consistently into two sublines for all excitation wavelengths and temperatures. In the resonance region of the Q_O and Q_V bands, the 0−1 and 0−0 resonances in the excitation profiles of the low-frequency (LF) sublines of ν_{19} and ν_{10} are red-shifted by (150 (30) cm^{-1} with respect to the sublines that are at higher frequencies (HF). In accordance with experimental and theoretical results, this indicates that the LF sublines of ν_{19} and ν_{10} result from a nonplanar conformer, whereas the HF sublines correspond to an almost planar conformer. The existence of this known conformational equilibrium in solution is further corroborated by the van't Hoff behavior of the intensity ratios I_{LF}/I_{HF} of the sublines of ν_{19} and ν_{10}. From the straight lines in the van't Hoff plot, we calculate that the nonplanar conformer in solution is energetically favored by about 3.0 kJ/mol.

Introduction

Metalloporphyrins exhibit a highly flexible tetrapyrrole skeleton which is able to adapt its conformation to different environments. Iron(II) protoporphyrin IX [Fe(PP)] derivatives, for instance, are significantly nonplanar when embedded in various heme proteins.[1] In most cases, the conformations of the hemes are found to be conserved within the proteins that belong to a single functional class.[1c] The degree of nonplanarity depends on the specific protein−heme interactions. Resonance Raman studies and molecular mechanics calculations[2,3a] indicate that the macrocycle of highly substituted porphyrins such as nickel(II) octaalkyltetraphenylporphyrins are nonplanar, resulting from the presence of at least two out-of-plane normal distortions of different symmetry types.[4] The predictions of molecular mechanics calculations are confirmed by crystallographic data such as the highly nonplanar nickel(II) octapropyltetraphenylporphyrin.[2a,3]

Molecular mechanics calculations of Shelnutt and coworkers[1c,2,3] on synthetic metalloporphyrins suggest that nonplanar distortions change bond lengths and angles of the macrocycle in a systematic way. For instance, increasing nonplanarity causes an increase of the $C_\alpha NC_\alpha$ angles of the pyrrole rings. Moreover, resonance Raman studies showed that these angles can be correlated to the frequency positions of some structure-sensitive Raman lines found in the region between 1300 and 1700 cm^{-1}. These correlations can be used for determining the degree of nonplanarity of porphyrins with unknown structures. The systematic investigations on a large variety of synthetic metalloporphyrins also revealed that nonplanarity may be caused by nonbonding interactions between peripheral substituents[2a,3] and by incorporation of too small central metal ions like nickel(II) into the porphyrin core.[2b] Hence, nonplanar conformations may result even in the absence of molecular crowding at the porphyrin periphery.

Nickel(II) octaethylporphyrin [Ni(OEP)], for instance, crystallizes in two triclinic A and B forms and one tetragonal C form (see Figure 1). In the triclinic forms, the macrocycles are flat but they differ with respect to the orientation of the eight ethyl groups.[5b,6] The tetragonal crystal structure,[5a] however, is strongly nonplanar. The opposite pyrrole planes are twisted by 32° (ruffling angle) with respect to an axes through the nitrogen atoms, leading to a ruffled conformation according to Scheidt and Lee's notation.[7] These different structures can be distinguished spectroscopically in that they give rise to different frequency positions in the Raman spectra, mainly the lines ν_3, ν_{11}, ν_2, ν_{19}, and ν_{10}. For example, in the single-crystal Raman spectra of Ni(OEP), the frequency differences between the triclinic forms and tetragonal form of the above structure-sensitive lines are $\Delta(A/B - C) \geq 7$ cm^{-1}.[6,8] On the other hand, in the Raman spectra of Ni(OEP) in organic solvents such as dichloromethane (CH_2Cl_2) or carbon disulfide (CS_2), these lines exhibit peak frequencies close to the values obtained for the two planar triclinic crystalline forms, but they also display shoulders at frequencies similar to those that are observed for the nonplanar tetragonal form. This observation was recently interpreted as an indication that Ni(OEP) in solution exists in at least two conformations: one with an almost planar and the other one with a nonplanar, probably ruffled structure.[2c,8,9]

Ni(OEP) can be considered as a suitable model compound for Fe(PP) because both have substituents at C_α positions which are similar and relatively small in size so that their macrocycles are not highly crowded. When Fe(PP) is embedded into a protein matrix, its biological function is modulated by protein−heme interactions. For instance, protonation of different amino acid groups leads to symmetry-lowering distortions of the porphyrin macrocycle changing its affinity for oxygen binding.[10]

* Correspondence should be sent to Reinhard Schweitzer-Stenner, FB1-Institut für Experimentelle Physik, Universität Bremen, P.O. Box 330440, 28334 Bremen, Germany; phone: +49-421-218-2509, FAX: +49−421−218−7318; E-mail: stenner@theo.physik.uni-bremen.de and stenner@alf.zfn.uni-bremen.de.

† Universität Bremen.

‡ Sandia National Laboratories.

§ University of New Mexico.

⊗ Abstract published in *Advance ACS Abstracts,* July 1, 1996.

S0022-3654(95)03303-X CCC: $12.00

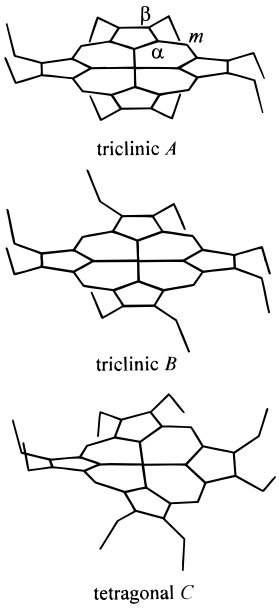

Figure 1. X-ray crystal structures of nickel(II) octaethylporphyrin in the triclinic forms, A[5b] and B,[6] and the tetragonal C form[5a] (hydrogen atoms are not shown). The three distinguishable carbons with respect to their positions are usually denoted by the symbols C_α, C_β , and C_m.

These structural changes require sufficient flexibility of the porphyrin macrocycle so that it can respond to even subtle changes in the protein matrix. It might be especially this high flexibility that has caused nature to select porphyrins as functional groups in various biological systems. It is therefore of principal interest to gain more insight into the interactions that influence the structure of porphyrins. Studies on metalloporphyrins in solution, for instance, can be expected to provide more knowledge about relevant intermolecular interactions and their dependencies on physical−chemical properties of the solvents.

In this work, we report resonance Raman spectra of Ni(OEP) in solution taken at excitation wavelengths from 430 to 580 nm and temperatures between 190 and 310 K. Because the shapes of the structure-sensitive lines ν_3, ν_{11}, ν_2, ν_{19}, and ν_{10} are clearly asymmetric, a detailed spectral analysis was employed, yielding a decomposition of their line shapes into two sublines. As a result of ambiguity of the fits and spectral crowding, only the most asymmetric and almost isolated lines, ν_{19} and ν_{10}, could be used for determining the spectral parameters of the corresponding sublines. We have measured the resonance excitation profiles (REPs) of these sublines which exhibit different resonance energies for both the Q_O- and Q_V-band excitation. This finding is in line with experimental results and predictions from quantum mechanical calculations.[1,3,9,11] Finally, measurements were carried out at various temperatures to determine the thermodynamic properties of the conformers that give rise to the sublines.

Materials and Methods

Preparation. Ni(OEP) was purchased from Sigma Chemie and *meso*-deuterated Ni(OEP) [Ni(OEP)-d_4] from Porphyrin Products. The materials were purified by liquid chromatography using CS_2 as the mobile phase (column 1(10 cm^2; Silicia 32-63, 60 A, ICN Biomedicals). The solvents CS_2 and CH_2Cl_2 (Aldrich) were from HPLC grade. The homogeneity of the samples was monitored by thin-layer chromatography using Kieselgel with fluorescence indicator F254 (Merck). The cystallization of the triclinic A and B forms and tetragonal C form of Ni(OEP) is described in earlier studies.[5,6]

UV−Vis Absorption Spectroscopy. The porphyrin concentrations in solutions were determined by measuring the UV−vis absorption spectra using a 10-mm quartz cell and a diode array spectrophotometer (Hewlett-Packard 8451 A). The extinction coefficients for Ni(OEP) in CS_2 and CH_2Cl_2 were determined by employing the published values for the same porphyrins in dioxane as a reference.[12] The band positions and extinction coefficients (in parentheses) for Ni(OEP) in CS_2 are 406 (170), 524 (12), and 558 nm (36 mM^{-1} cm^{-1}), and in CH_2Cl_2, 392 (202), 516 (12), and 552 nm (34 mM^{-1} cm^{-1}). The accuracy is 10% for the extinction coefficients and ±2 nm for the absorption band positions. In the Raman experiment, the porphyrin concentrations were in the range between 0.5 and 2 mM.

Resonance Raman Spectroscopy. The resonance Raman spectra were recorded by using two Raman apparatuses. An excimer pumped dye laser system was used to determine the REPs of the structure-sensitive lines of Ni(OEP) in solution. The solution Raman spectra at different temperatures and the single-crystal Raman spectra at room temperature were obtained by using a CW laser system.

Excimer Punped Dye Laser System. The polarized Raman spectra of Ni(OEP) at different excitation wavelengths were measured at room temperature with an excimer (Lambda EMG53MSC) pumped dye laser (Lambda FL2001). All measurements were carried out in backscattering geometry. The spectra were recorded with excitation wavelengths from 430 to 580 nm with an average spectral distance of 3 nm that cover the resonance and preresonance region of Q_O- and Q_V-band excitation. The pulse energy was 1 mJ at a 200-Hz repetition rate and a pulse length of 10 ns. Thus, an average power of 200 mW was provided. By using two pinholes and a cylindrical lens of 50-cm focal length, the scattered light was filtered and focused onto the sample placed in a cylindrical rotating quartz cell. Rotation of the Raman cell at 50 Hz prevented local heating of the absorbing sample. The scattered light was collected and imaged onto the entrance slit of the spectrometer. Polarized spectra were measured by passing the scattered light through a polarization filter (Spindler & Hoyer) oriented parallel (∥) or perpendicularly (⊥) to the incident laser polarization followed by a scrambler in front of the spectrometer. The scattered light was dispersed by a Czerny−Turner monochromator (Spex 1877) equipped with a grating with 1200 grooves/mm. The geometrical slit S was adjusted to 50 μm. A preceding double monochromator was used as a filter to suppress stray light. The scattered light was detected by a CCD camera (Photometric series 200, 5700051 version 6.0) cooled with liquid nitrogen. The collected data were stored in computer.

In order to obtain the true Raman line shapes, the observed line shapes were deconvoluted with the slit function of the spectrometer.[4] This spectral slit functions were determined by recording the spectral lines of several pencil lamps (e.g., neon, krypton, etc.) and can be described well by Gaussian functions. The line width (spectral slit widths) of the spectral slit function depends on the excitation wavelengths which are, for instance, 2.5 cm^{-1} at 560 nm and 5.3 cm^{-1} at 420 nm when using a 50-μm slit width. (It has to be noted that the device-limited spectral resolution of the CCD array is about ±1 cm^{-1}, which is smaller than the spectral slit widths in the experiment.)

The frequency calibration of the Raman spectra was carried out by using the intensive 653-cm^{-1} solvent line from CS_2 which also served as an internal standard for determining the REPs of the porphyrin Raman lines. The obtained REPs were corrected for absorption as described in previous study.[13] The estimated

errors of the observed line positions at different excitation wavelengths are ± 1 cm^{-1}.

CW Laser System. Measurements at different temperatures of Ni(OEP) in solution and its single-crystal spectra at room temperature were carried out with CW excitation provided by an argon ion laser (Spectra-Physics, Model 2020-05) or an argon laser pumped dye laser (Spectra-Physics, Model 375). The measurements were again performed with backscattering geometry. By using a cylindrical lens of 10-cm focal length, the linear polarized laser beam was focused onto the sample placed in a low-temperature cell consisting of a cylindrical quartz cuvette surrounded by a copper block. The cell was mounted onto the cold finger of a closed cycle cryostat (Leybold, ROK 10-300), and its temperature was regulated by a controller unit (Leybold, Variotemp HR1). The estimated errors of the temperature of the sample are ± 5 K. The single crystals of Ni(OEP) were placed between two thin quartz slides. The spectra were detected by mounting the sample holder and the reference (pencil lamps) in front of the camera objective. In contrast to the solution spectra, the cylindrical lens was defocused and the laser power was less than 20 mW to avoid strong local heating of the single crystals. No sample decomposition was observed by checking the sample integrity of the single crystals under the microscope and by comparing the Raman signal before and after the measurements.

The scattered light was collected and imaged on the entrance slit of the spectrometer (Spex 1401) equipped with a cooled photomultiplier (RCA, type C31034-02) and photon counting electronics (Ortec 9302, 9320). The data were stored in computer which also controls the photon counter and the motor of the spectrometer. Polarized Raman spectra were observed by using a polarization filter as analyzer (Spindler & Hoyer) placed in front of the entrance slit of the spectrometer followed by a scrambler.

The spectral slit width of the Czerny−Turner double monochromator used was calculated by employing the following equation:[14]

$$\tilde{s} = \frac{S\nu d}{4mf}\sqrt{4\nu^2 - (m/d)^2} \qquad (1)$$

S is the geometric entrance (and exit) slit width, $\tilde{\nu}$ the absolute wavenumber position, and f the collimator focal length of the spectrometer. d is the spacing of the gratings and m the diffraction order. The spectrometer used has $d = 1/1200$ mm, $m = 1$, and $f = 850$ mm, which for $S = 100$ μm and $\lambda = 1/\nu^2 = 413$ nm (at the Rayleigh line position of the excitation wavelength) gives a spectral slit width of $\tilde{s} = 2.8$ cm^{-1}. The experimentally determined spectral slit functions, which were obtained by using the spectral lines of krypton and argon pencil lamps, can be described by Gaussians ($S < 100$ μm) or triangularly shaped functions ($S > 100$ μm). The maximal deviations of the experimentally determined spectral slit widths to the calculated ones (eq 1) were less than 5%.

The frequency calibration of the solution spectra at different temperatures and the single-crystal spectra at room temperature was carried out by using suitable spectral lines of krypton and argon pencil lamp (Oriel). The light from these lamps was directed onto the spectrometer slit for the short time that is necessary to record the spectral lines. The linearity of the spectrometer was checked by measuring the positions of spectral lines between 10 000 and 30 000 cm^{-1}. The deviations from linearity were ± 1 cm^{-1} per 5000 cm^{-1}. The estimated errors of the observed line positions are 0.5 cm^{-1} unless it is explicitly stated.

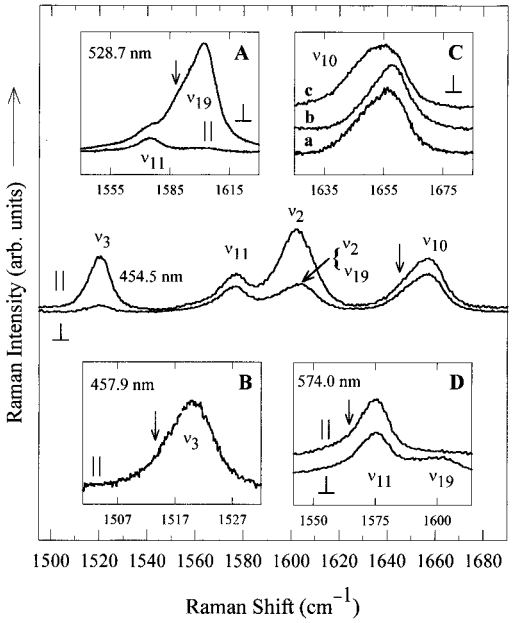

Figure 2. Resonance Raman spectra with 454.5-nm excitation in the 1300−1700-cm^{-1} region of Ni(OEP) in CH_2Cl_2 taken with a CW laser (middle part). Symbols || and ⊥ denote the parallel and perpendicular polarization. The arrows indicate the asymmetry of the line shape. Insets: (A) 528.7 nm; (B) 457.9 nm; (C) 457.9 nm (a), 547.3 nm (b), 564.2 nm (c); (D) 574.0 nm. Typical conditions: 50 mW, 1.5 mM, spectral slit widths about 2 cm^{-1}.

Curve Fitting. The spectra at different excitation wavelengths were analyzed using a novel line shape analysis program called MULTIFIT.[15] The observed line shapes were deconvoluted with the above spectrometer slit functions which were approximated for both apparatuses by Gaussian functions with line widths. The Raman spectra at different excitation wavelengths were consistently analyzed. In other words, the observed spectra were subjected to a global fit in which each Raman line has identical line widths and frequency positions at all excitation wavelengths. Therefore, we can eliminate ambiguities in the line shape analysis. The Raman spectra obtained at different temperatures were also analyzed using the MULTIFIT program, allowing the observed line shapes to be fit with Lorentzian, Gaussian, or Voigtian lines. Upon analyzing the Raman spectra at different excitation wavelengths and temperatures, the above procedure reveals that some Raman lines appear as doublets or even triplets, and the components of such a multiplet are designated as sublines throughout this work. The spectral slit width and the width (or half-widths) of the Raman line are defined by the full width at half-maximum, and the Raman line widths given in the text are all corrected for the spectrometer slit function. Finally, a linear function was employed to fit the background intensity.

Results

Polarized Raman Spectra of the Structure-Sensitive Lines. The middle part of Figure 2 displays an overview of the polarized resonance Raman spectra of Ni(OEP) in CH_2Cl_2 taken at room temperature. The spectra cover the region of the structure-sensitive lines ν_3 (A_{1g}), ν_{11} (B_{1g}), ν_2 (A_{1g}), ν_{19} (A_{2g}), and ν_{10} (B_{1g}) which appear at peak frequencies 1520, 1575, 1601, 1603, and 1656 cm^{-1}, respectively. Similar spectra of Ni(OEP) were observed with CS_2 as solvent. The assignment, labeling, and symmetry of these Raman lines are based on the recent normal mode analysis of Ni(OEP).[16] According to the potential energy distribution, the vibrational energy of the modes ν_{11} and ν_2 is mainly localized in the $C_\beta C_\beta$ bond. The modes

ν_{10} and ν_{19} are primarily $C_\alpha C_m$ stretching, and ν_3 results from almost equal contributions of $C_\beta C_\beta$ and $C_\alpha C_m$ stretchings.

Raman lines resulting from modes of different symmetry can be selectively enhanced by using appropriate excitation wavelengths. The polarized spectra in the middle part of Figure 2 were recorded with 454.5-nm excitation wavelength. This ensures a predominant enhancement of polarized lines (ν_3 and ν_2) owing to comparatively strong Franck−Condon coupling within the strongly dipole allowed B states.[13] At the above excitation, the intensity of the depolarized B_{1g} lines (ν_{11} and ν_{10}) arises from intrastate Jahn−Teller coupling within the B states.[10,13,17,18] Insets A−D in Figure 2 present an enlarged view of the structure-sensitive lines. Inset A shows the lines ν_{11} and ν_{19} recorded with 528.7-nm excitation wavelength that provides Q_V-band resonance enhancement, in particular for ν_{19}.[18] The inversely polarized line ν_{19} does not appear in the parallel polarized Raman spectrum because of its nearly infinite depolarization ratio [ρ(obsd) > 20]. The other Raman lines investigated show (ρ values of 0.125 and 0.75 for A_{1g} and B_{1g} or B_{2g} modes, respectively, indicating that the molecular symmetry of Ni(OEP) in solution is D_{4d}, D_4, C_{4v}, or D_{2d}.[19,20] Even eyeballing of the spectrum reveals that the line ν_{19} is highly asymmetric. The polarized line ν_2, which strongly overlaps with ν_{19}, is relatively weak in Q-band excitation. The depolarized line ν_{11} appears in the parallel and perpendicularly polarized spectrum. This line is more isolated with Q_O-band excitation (574 nm, inset D).[13,18] Inset B displays the isolated line ν_3 observed with 457.9-nm excitation wavelengths. Inset C displays the shape of the line ν_{10} recorded with three different excitation wavelengths: (a) 457.9, (b) 547.3, and (c) 564.2 nm. Apparently, the peak frequency and the line shape change by using different excitation wavelengths, indicating that the line ν_{10} is composed of at least two sublines which have different resonance positions of their REPs.

Ambiguity of the Fits for the Lines ν_3 and ν_{11} and Spectral Crowding in the ν_2 Region. Because of the apparent asymmetric shape of the above structure-sensitive Raman lines ν_3, ν_{11}, ν_2, ν_{19}, and ν_{10}, we first tried to decompose consistently each line at different excitation wavelengths and temperatures into two sublines (*vide infra*). However, an unambiguous fitting of the data is difficult due to strong correlations between the free parameters and spectral crowding. The lines ν_3 and ν_{11} in both solvents and the line ν_{19} of Ni(OEP) in CH_2Cl_2 do not yield unambiguous spectral parameters. Although the lines ν_3 and ν_{19} are clearly asymmetric (see Figure 2), it was not possible to obtain reliable spectral parameters for these lines. Similarly, the line ν_{11} can be described well by one Gaussian or Lorentzian. Moreover, the line ν_2 in both solvents is contaminated by at least one underlying line which can be shown by comparing the solution spectra with the single-crystal spectra (Figure S1 in the supporting information) as well as the Raman spectra from Ni(OEP)-d_4 (deuterated at the *meso* positions) at different temperatures (Figure S2 in the supporting information).

Thus, the first inspection of the data reveals that only the lines ν_{19} and ν_{10} of Ni(OEP) in CS_2 and the line ν_{10} in CH_2Cl_2 reveal reliable fits and can be used to evaluate the Raman excitation profiles and the temperature dependence of their sublines. The reduced χ^2 values for all these fits are in the confidence region between 1 and 2, indicating that they are satisfactory and statistically meaningful.[22] In the following, we confine our analysis to the REPs and temperature dependence of the sublines of ν_{19} and ν_{10}.

Resonance Excitation Profiles of the Structure-Sensitive Lines ν_{19} and ν_{10}. Figure 3 (panel A) shows the line ν_{19} in the perpendicularly polarized spectrum taken with 552-nm and 564-nm excitation wavelengths in which the intensity contribution of the line ν_{11} is removed by the following procedure. The corresponding parallel polarized spectrum was multiplied by 0.75 and then used to subtract the line ν_{11} from the observed perpendicularly polarized spectrum {$I_\perp$(shown) = $I_\parallel$(obsd) − [$I_\parallel$(obsd)0.75]}. This can be carried out because the intensity contribution of the line ν_2 (A_{1g}) is negligible for the above excitation wavelengths. After the subtracting procedure, the shape of the line ν_{19} is clearly asymmetric, and the analysis reveals two sublines labeled as low frequency (LF) ν_{19}^{LF} and high frequency (HF) ν_{19}^{HF}. The remaining line labeled as ν_{19}* is weak (or absent) in the corresponding spectra recorded with CW excitation. In the experiment with pulse excitation, the intensities (area of the Raman lines) increase quadratically with the incident laser power. This suggests that it results from optical pumping into the excited states of nickel(II).[21] Figure 3 (panel B) shows the line ν_{10} in the parallel polarized spectrum of Ni(OEP) in CS_2 excited with 552-nm and 568-nm wavelengths provided by the excimer pumped dye laser. The two sublines are designated in the figure by the symbols ν_{10}^{LF} and ν_{10}^{HF}. Moreover, a third line ν_{10}* is necessary (not clearly seen in this Figure) to fit the Raman spectra at different excitation wavelengths that may also result from a photoexcited state.[21]

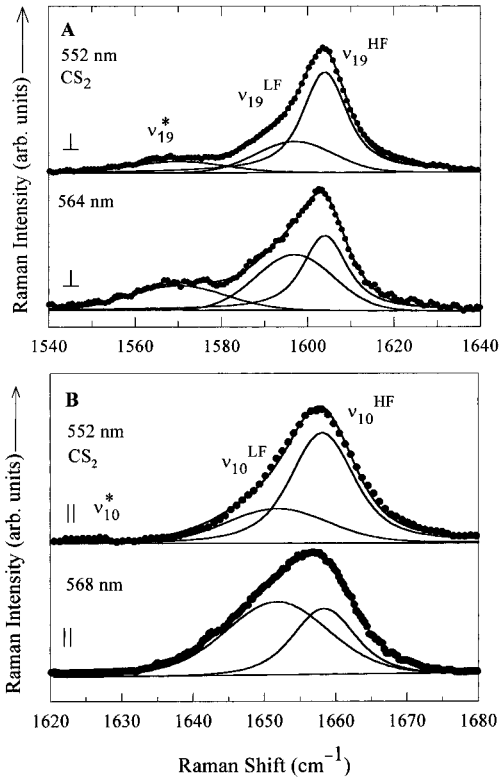

Figure 3. Resonance Raman spectra of Ni(OEP) at different excitation wavelengths in CS_2 taken with the excimer pumped dye laser. Panel A shows the perpendicularly polarized spectra of the line ν_{19} {$I_\perp$(shown) = $I_\perp$(obsd) − [$I_\parallel$(obsd)0.75]} and panel B the parallel polarized spectra (||) of the line ν_{10}. Typical conditions: 50 mW, 1 mM, spectral slit widths about 3 cm^{-1}.

Taken together, the curve fitting procedure reveals that the asymmetric shapes of the structure-sensitive lines ν_{19} and ν_{10} at different excitation wavelengths can be described well by two sublines. All LF sublines are rather broad Gaussians, whereas the corresponding HF sublines are Voigtians. It has to be noted that the spectral parameters listed in Table 1 to fit the Raman line shapes were kept constant for all excitation wavelengths used and are therefore self-consistent. For both lines, the intensity ratios of the LF and HF subline change

TABLE 1: Frequency Positions (in cm^{-1}) and Widths (Γ in cm^{-1}) of the High-Frequency (HF) and Low-Frequency (LF) Sublines of ν_{19} and ν_{10} of Ni(OEP) in CS_2 Solution Derived from the Consistent Analysis of the Raman Spectra Measured at Room Temperature with the Excimer Pumped Dye Laser[a]

	LF subline (Gaussian)[b]		HF subline (Voigtian)		
mode	position	Γ_G[c]	position	Γ_L[c]	Γ_G[c]
ν_{19} (A^{2g})	1597	21	1604	9	5
ν_{10} (B_{1g})	1652	15	1659	8	6

[a] Estimated errors of the frequency positions and linewidths are ± 1 cm^{-1} and 10%, respectively. [b] In the curve fitting procedure, the Gaussian line widths are assumed to be temperature-independent (see text). [c] Indexes G and L denote the Gaussian (corrected for the spectrometer function) and Lorentzian contributions to the width of the Raman line.

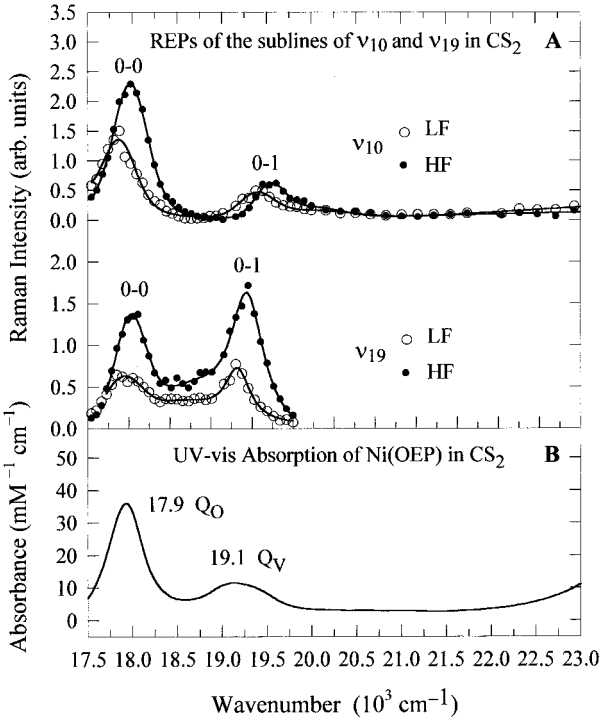

Figure 4. Upper panel (A) shows the resonance Raman excitation profiles of the low- (LF) and high-frequency sublines (HF) ν_{19} (A_{2g}) and ν_{10} (B_{1g}) for Ni(OEP) in CS_2 based on the decomposition described in the text. The spectral parameters used for the decomposition are listed in Table 1. Lower panel B displays the UV−vis absorption spectrum showing the Q_V and Q_O band of Ni(OEP) in CS_2.

significantly when using different excitation wavelengths. This indicates that the REPs of the corresponding sublines must be different.

Figure 4 displays the REPs of the LF and HF sublines of ν_{19} and ν_{10} in the Q_O- and Q_V-band region. The 0−0 and 0−1 resonances in the REPs of the LF sublines of ν_{19} and ν_{10} are obviously red-shifted by 150 ± 30 cm^{-1} with respect to the corresponding REPs of the HF sublines. This explains the wavelength dependence of the Raman line shapes.

Temperature Dependence of the Lines ν_{19} and ν_{10}. Figure 5 (panels A and B) depicts the shapes of the lines ν_{19} and ν_{10} measured at 310 and 193 K in CS_2 solution; the shape of the line ν_{10} for Ni(OEP) in CH_2Cl_2 is also shown in Figure 5 (panel C). The polarized spectra were recorded with 454.5-nm (ν_{10}) and 528.7-nm excitation (ν_{19}) provided by an argon ion laser. These lines exhibit a noticeable temperature dependence of both their line shapes and frequency positions.

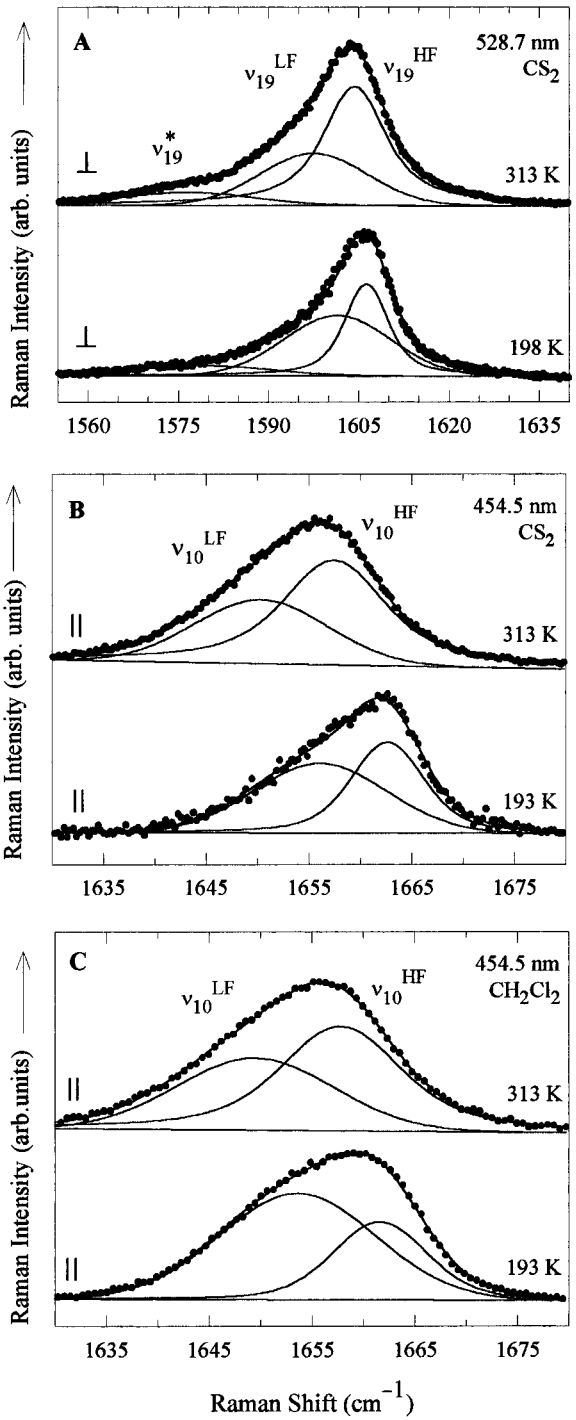

Figure 5. Resonance Raman spectra of Ni(OEP) in solution at high and low temperature taken with a CW laser and the decomposition of the asymmetric shapes of the structure-sensitive lines ν_{19} and ν_{10} into two sublines (fitting procedure is described in text). Panels: (A) 528.7 nm, CS_2; (B) 454.5 nm, CS_2; (C) 454.5 nm, CH_2Cl_2. Symbols || and ⊥ denote the parallel and perpendicular polarization. Typical conditions: 50 mW, 1.5 mM, spectral slit widths 2.1 cm^{-1} (454.5 nm) and 1.5 cm^{-1} (528.7 nm).

These lines taken at temperatures between 193 and 310 K were subjected to the fitting procedure which was also used for the spectra obtained from the excimer pumped dye laser. In other words, each line at different temperature was also decomposed into two sublines. The frequency positions and Lorentzian widths of the sublines were used as free parameters in the fitting procedure. However, the Gaussian widths of the HF sublines (pure Gaussians) and the LF sublines (Voigtians) are assumed to be temperature-independent because they

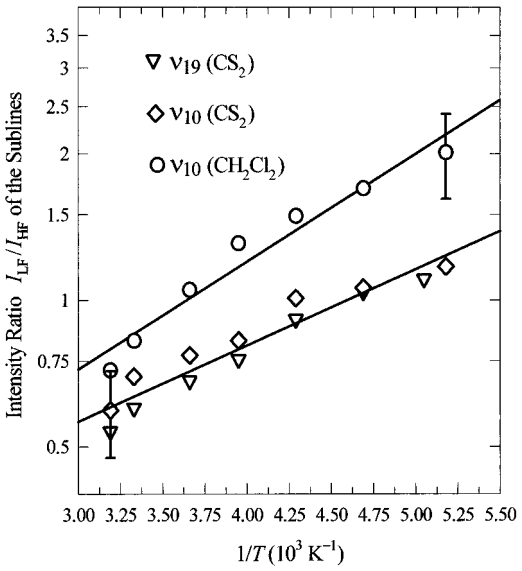

Figure 6. Van't Hoff plots of the intensity ratios I_{LF}/I_{HF} of the sublines of ν_{19} and ν_{10}. The solid lines are the calculated values according to the thermodynamic model resulting from a fit to the data with eq 2. The thermodynamic parameters are listed in Table 2. The bars illustrate the maximal errors in determining the ratios.

probably arise from inhomogenous broadening. We cross-checked this assumption by using two alternative analyses to estimate the influence of the temperature dependence of the intensity ratios of the sublines of ν_{19} and ν_{10}. First, the Gaussian widths of the LF sublines were allowed to depend on temperature. In this case, we found good reproduction of the temperature dependence of the intensity ratios I_{LF}/I_{HF} (*vide infra*). The second alternative invokes Lorentzian shapes for the sublines and also reveals similar results; however, these fits are significantly reduced in quality in comparison to the spectral model which uses Gaussian and Voigtian line shapes.

The curve fitting procedure clearly reveals that the spectral parameters of the sublines of ν_{19} and ν_{10} are temperature-dependent. The van't Hoff plot of their intensity ratios is shown in Figure 6. The ratios I_{LF}/I_{HF} of the sublines of ν_{19} and ν_{10} become larger as the temperature is lowered. As shown in Figure 7, the frequency positions of the sublines increase linearly with decreasing temperature, whereas the Lorentzian widths of the LF sublines decrease. [The corresponding Gaussian widths of the HF sublines (pure Gaussians) and LF sublines (Voigtians) are temperature-independent as we assumed in the curve fitting procedure.]

Additionally, it has to be noted that other Raman lines (ν_5, ν_{30}, ν_{13}, ν_4, ν_{29}) can be described well with single Lorentzian (or Voigtian). The temperature dependence of their *observed* line widths is similar to the HF sublines (Voigtians), but their frequency positions do not change much with temperature. The Lorentzian widths of the Raman lines ν_5 (A_{1g}) at 1139, ν_{30} (B_{2g}) at 1159, ν_{13} (B_{1g}) at 1220, ν_4 (A_{1g}) at 1383, and ν_{29} (B_{2g}) at 1409 cm^{-1} are similar and change from approximately 7.5 (298 K) to 5.5 cm^{-1} (190 K). Their corresponding frequency upshifts are 1.6 (ν_5), 0.1 (ν_{30}), 0.1 (ν_{13}), 1.1 (ν_4), and 1.3 cm^{-1} (ν_{29}). The accuracy is 10% for the Lorentzian line widths and (0.5 cm^{-1} for the frequency differences.

Discussion

The decomposition of the Raman lines ν_{19} and ν_{10} of Ni(OEP) in CS_2 and the line ν_{10} in CH_2Cl_2 yields two sublines with different widths. The intensity ratios of the sublines depend on the excitation wavelength and temperature. The LF sublines

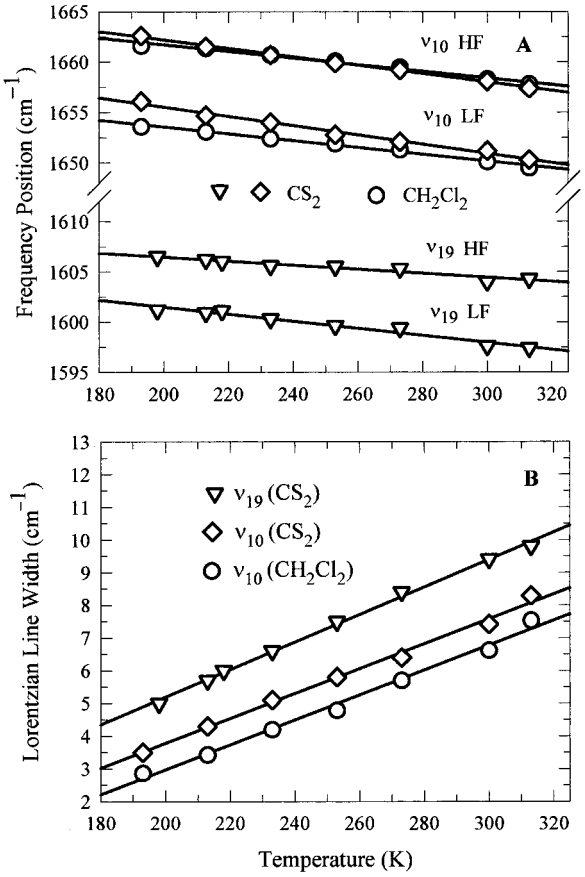

Figure 7. Temperature dependence of the frequency position (panel A) of the LF and HF sublines and Lorentzian linewidths (panel B) of the LF sublines of ν_{19} and ν_{10}. The Gaussian widths for the high-frequency (HF) sublines (pure Gaussians) and low-frequency (LF) sublines (Voigtians) are assumed to be temperature-independent (see text).

are Gaussians and comparatively broad, whereas the HF sublines are best fitted by Voigtians with strong Lorentzian contributions. Additionally, the frequency positions and the Lorentzian line widths depend on temperature. Figure 6 displays the van't Hoff plots of the intensity ratios of the sublines of ν_{19} and ν_{10} for Ni(OEP) in CS_2. For comparison, the data in CH_2Cl_2 for the line ν_{10} are also shown in Figure 6. Figure 7 illustrates the temperature dependence of their frequency positions and Lorentzian line widths.

In view of earlier Raman studies[2−4,11,23] on highly substituted metalloporphyrins and on Ni(OEP) in crystalline forms and solutions,[2c,6,8,9] it is known that nonplanar distortions of the macrocycle like ruffling or saddling cause a downshift of the frequencies for the Raman lines ν_3, ν_{11}, ν_2, ν_{19}, and ν_{10}. Furthermore, Shelnutt and co-workers[3] reported recently that nonplanar distortions cause a red shift of the UV−vis absorption bands. As a consequence, the maxima of the REPs of the LF sublines of ν_{19} and ν_{10} are expected to be red-shifted with respect to those of the corresponding HF sublines. As can be seen from Figure 4, this is indeed the case. Hence, the LF sublines of ν_{19} and ν_{10} come from a nonplanar conformer, whereas the corresponding HF sublines result from a conformer with a more planar macrocycle.

In view of this result, the thermodynamic model for interpreting the temperature dependence of the intensity ratios consists of two states: an almost planar (P) and a nonplanar, probably ruffled, conformer (R). If the occupation numbers n_R and n_P of the states are proportional to the Raman intensities of the high-frequency (I_{HF}) and low-frequency sublines (I_{LF}), then the

TABLE 2: Thermodynamic Parameters[a] Derived from the van't Hoff Plots of the Intensity Ratios of the Sublines of ν_{19} and ν_{10} (Raman Cross Sections Are Assumed To Be Identical for the Two Conformers)

mode	$\Delta H_{R,P}$ (kJ mol^{-1})	$\Delta S_{R,P}$[b] (J mol^{-1} K^{-1})
CS_2 (ν_{19}, ν_{10})	−2.8	−13.0
CH_2Cl_2 (ν_{10})	−3.5	−13.5

[a] Estimated errors of the entropy and enthalpy are 20%. [b] Values are physically not very accurate because the thermodynamic model assumes that the Raman cross sections are identical for the conformers.

intensity ratios of the sublines can be described by the following resonance Raman (modified) van't Hoff equation:

$$\frac{I_{LF}}{I_{HF}} = \frac{\sigma_R}{\sigma_P}\frac{n_R}{n_P} = \frac{\sigma_R}{\sigma_P}\exp\left(-\frac{\Delta G_{R,P}}{RT}\right) \quad (2)$$

σ_P and σ_R are the Raman cross sections of the two conformers, T the absolute temperature, and R the universal gas constant. $\Delta G_{R,P}$ is the Gibbs free energy difference between the two states defined by the Gibbs−Helmholtz equation:

$$\Delta G_{R,P} = \Delta H_{R,P} - T\Delta S_{R,P} \quad (3)$$

The thermodynamic parameters $\Delta H_{R,P}$ and $\Delta S_{R,P}$ are the enthalpic and entropic difference between the two states. According to eq 2, the two-state model predicts straight lines in the van't Hoff plots of the intensity ratios.

The thermodynamic parameters of the two-state model, which were obtained from the fits to the data in Figure 6 are listed in Table 2. At this point, it has to be mentioned that the entropic part also includes the degeneracy of each state. In other words, it describes the number of energetically identical, nondistinguishable states. In the ruffled conformation, for instance, the opposite pyrrole planes can be twisted counter-clockwise or clockwise with respect to an axes through the nitrogen atoms. Hence, the degeneracy factor of the ruffling distortion is 2. On the other hand, the degeneracy factor of the planar macrocycle is 1. Obviously, the exact degeneracy factors depend on the specific distortions of the macrocycle as well as the possible arrangements of the peripheral substituents (number of permutations). The entropic values listed in Table 1 are calculated by assuming that the Raman cross sections of the corresponding sublines are identical. This assumption, however, is known to be incorrect,[24] and consequently, the interpretation of the $\Delta S_{R,P}$ value is complicated. Differences between Raman cross sections are brought about by the above-mentioned shift of the resonance energies as well as by direct changes of the vibronic coupling parameters. The latter case is in particular relevant for ν_{10} because the resonance excitation of B_{1g} modes is complicated due to interferences between different intra- and interstate vibronic coupling processes.[13]

In summary, the thermodynamic model accounts for the REPs and the temperature dependence of the intensity ratios of the sublines of ν_{19} and ν_{10}. The two sublines of ν_{10} and ν_{19} result from conformers with planar and nonplanar macrocycles. The nonplanar conformer is energetically favored by about 3.5 and 2.8 kJ/mol in CH_2Cl_2 and CS_2 solutions, respectively. In accordance with experimental and theoretical results, the maxima of the excitation profiles of the LF sublines are red-shifted with respect to the profiles of the HF sublines.

The above results are further substantiated by UV−vis absorption data reported in the following paper in this issue.[25] The B band of Ni(OEP) can be decomposed into two subbands, and their intensity ratios at different temperatures also indicate a stabilization of the nonplanar conformer at low temperatures.

Structural Dynamics and Molecular Mechanics Calculations. Our results contradict conclusions drawn from earlier Raman experiments. Czernuszewicz and co-workers[8] have compared Raman spectra on crystallized and dissolved Ni(OEP) at different temperatures. They argued that the upshift of the frequency position of the line ν_{10} with decreasing temperature indicates that a more planar conformation is stabilized at low temperatures. This interpretation is based on the assumption that nonplanarity is mainly caused by the occupation of higher vibrational levels of out-of-plane modes located at lower frequencies rather than associated with a minimum in the Gibbs free energy landscape of the macrocycle. The potential of the out-of-plane modes was assumed to be anharmonic. This model would imply that the shape of those Raman lines, whose frequency positions are sensitive to nonplanar distortions, should become more symmetric at low temperatures due to the depopulation of higher vibrational states. This is in contradiction to our data because the asymmetry of the Raman lines investigated is even higher at low temperatures (see Figure 5).

Munro and co-workers[26] reported molecular mechanics calculations for various metalloporphyrins. For Ni(OEP), they predict an enthalpic stabilization of the planar rather than the nonplanar conformer. Also, earlier calculations by Shelnutt and co-workers[2a] gave the result that the planar conformation is energetically favored. However, these calculations do not include the crystal packing and solvent−porphyrin interactions which can also have a significant influence of the energy landscape of the porphyrin macrocycle. With recent improvements in the Shelnutt's force field parameters,[24] the molecular mechanics calculations, however, predict both planar and ruffled forms of Ni(OEP) and even the experimentally observed difference in energy between planar and nonplanar conformation of nickel(II) *meso*-tetraphenylporphyrin [Ni(TPP)] and nickel(II) *meso*-5,15-diphenylporphyrin [Ni(diPP)] is reasonable.[24]

Summary

The existence of discrete conformations of Ni(OEP) in solution accounts for the asymmetric shapes of the structure-sensitive Raman lines and their change with temperature. The two sublines of the lines ν_{19} and ν_{10} result from conformers whose macrocycles differ in terms of nonplanarity. In the thermodynamic model, the nonplanar structure is energetically favored by about 3.0 kJ/mol. The resonance excitation profiles of these sublines provide conclusive evidence that nonplanar distortions cause a red shift of the Q-band resonance positions and decrease the Raman line intensity.

Acknowledgment. W.J. and G.K. thank the University of Bremen for a Graduate Fellowship. W. J. is a recipient of an Associated Western Universities Postdoctoral Fellowship. This work was supported by U.S. DOE Contract DE-AC04-94DP85000 (J.A.S.).

Supporting Information Available: Figure S1 shows the single-crystal Raman spectra with 457.9-nm excitation wavelength of the three crystalline forms of Ni(OEP). The Raman spectra were taken between 1500 and 1700 cm^{-1}. Local heating of the samples is avoided at this excitation wavelength while enhancement of the structure-sensitive Raman lines ν_3, ν_{11}, ν_2, and ν_{10} (the excitation wavelengths used for the single-crystal Raman spectra does not enhance the line ν_{19}) is obtained. Their frequency positions and frequency differences are listed in Table S1 and are in good agreement with earlier data,[6,8] indicating

that the samples are in the right single-crystalline forms. Since the single crystal of Ni(OEP) contains only one (crystal) conformer, we expect narrow widths and symmetric shapes for the single-crystal Raman lines. It can be seen from Figure S1 that the lines ν_3 and ν_{10} are symmetric and narrow but ν_2 is not. In the triclinic forms, the line ν_2 is clearly asymmetric caused by an unassigned line at a fitted position of about 1601 cm^{-1}.[27] The asymmetric shapes of the line ν_2 in the triclinic forms also appear at 413.1-nm excitation wavelength (data not shown) and are well reproducible for both excitation wavelengths. Moreover, the spectral crowding in the ν_2 region is further corroborated by the Raman spectra from deuterated Ni(OEP) in solution. Figure S2 shows the Raman spectra between 1540 and 1680 cm^{-1} of Ni(OEP)-d_4 (*meso*-d_4) and the naturally occurring Ni(OEP) in CS_2 solution. These spectra were taken with 413.1-nm excitation at 290 and 200 K under the same experimental conditions. At room temperature, the line ν_2 clearly becomes narrower and less asymmetric upon deuteration, whereas the shape of the lines ν_{10} is still broad and asymmetric. On the other hand, the shape of the line ν_2 from naturally occurring Ni(OEP) is strongly temperature-dependent, whereas the line ν_2 for Ni(OEP)-d_4 does not change much. This indicates that the temperature dependence of the line ν_2 is not mainly due to a change in the occupation number of the two conformers.[28] Taken together, both the single-crystal spectra of naturally occurring Ni(OEP) and the spectra from its isotopomer Ni(OEP)-d_4 clearly demonstrate spectral crowding in the ν_2 region. Table S1 gives the frequency positions and differences of the structure-sensitive lines of Ni(OEP) in the single crystals. (4 pages.) See any current masthead page for ordering information.

References and Notes

(1) (a) Shaanan, B. *J. Mol. Biol.* **1983**, *171*, 31. (b) Barkigia, K. M.; Chantranupong, L.; Smith, K. M.; Fajer, J. *J. Am. Chem. Soc.* **1988**, *110*, 7566. (c) Hobbs, J. D.; Shelnutt, J. A. *J. Protein Chem.* **1995**, *14*, 19. (c) Jentzen, W.; Shelnutt, J. A. *J. Am. Chem. Soc.*, submitted for publication.

(2) (a) Shelnutt, J. A.; Medforth, C. J.; Berber, M. D.; Barkigia, K. M.; Smith, K. M. *J. Am. Chem. Soc.* **1991**, *113*, 4077. (b) Shelnutt, J. A.; Majumder, S. A; Sparks, L. D.; Hobbs, J. D.; Medforth, C. J.; Senge, M. O.; Smith, K. M.; Miura, M.; Quirke, J. M. E. *J. Raman Spectrosc.* **1992**, *23*, 523. (c) Anderson, K. K.; Hobbs, J. D.; Luo, L.; Stanley, K. D.; Quirke, J. M. E; Shelnutt, J. A. *J. Am. Chem. Soc.* **1993**, *115*, 12346. (d) Hobbs, J. D.; Majumder, S. A.; Luo, L.; Sickelsmith, G. A.; Quirke, J.M. E.; Medforth, C. J.; Smith, K. M.; Shelnutt, J. A. *J. Am. Chem. Soc.* **1994**, *116*, 3261.

(3) (a) Jentzen, W.; Simpson, M. C.; Hobbs, J. D.; Song, X.; Ema, T.; Nelson, N. Y.; Medforth, C. J.; Smith, K. M.; Veyrat, M.; Mazzanti, M.; Ramasseul, R.; Marchon, J.-C.; Takeuchi, T.; Goddard, III, W. A.; Shelnutt, J. A. *J. Am. Chem. Soc.* **1995**, *117*, 11085. (b) Song, X.; Jentzen, W.; Jia, S.; Jaquinod, L.; Nurco, D. J.; Medforth, C. J.; Smith, K. M.; Shelnutt, J. A. *J. Am. Chem. Soc.*, submitted for publication.

(4) Stichternath, A.; Schweitzer-Stenner, R.; Dreybrodt, W.; Mak, R. S. W.; Li, X.-Y.; Sparks, L. D.; Shelnutt, J. A.; Medforth, C. J.; Smith, K. M. *J. Phys. Chem.* **1993**, *97*, 3701.

(5) (a) Meyer, E. F. *Acta Crystallogr., Sect. B* **1972**, *28*, 2162. (b) Cullen, D. L.; Meyer, E. F. *J. Am. Chem. Soc.* **1974**, *96*, 2095.

(6) Brennan, T. D.; Scheidt, W. R.; Shelnutt, J. A. *J. Am. Chem. Soc.* **1988**, *110*, 3919.

(7) Scheidt, W. R.; Lee, Y. J. *Struct. Bonding (Berlin)* **1987**, *64*, 1.

(8) Czernuszewicz, R. S.; Li, X.-Y.; Spiro, T. G. *J. Am. Chem. Soc.* **1989**, *111*, 7024.

(9) Alden, R. G.; Crawford, B. A.; Doolen, R.; Ondrias, M. R.; Shelnutt, J. A. *J. Am. Chem. Soc.* **1989**, *111*, 2070.

(10) Schweitzer-Stenner, R. *Q. Rev. Biophys.* **1989**, *22*, 381.

(11) Sparks, L. D.; Medforth, C. J.; Park, M.-S., Chamberlain, J. R.; Ondrias, M. R.; Senge, M. O.; Smith, K. M.; Shelnutt, J. A. *J. Am. Chem. Soc.* **1993**, *115*, 581.

(12) Furhop, J. H.; Smith, K. M. In *Laboratory methods in porphyrins and metalloporphyrin research*; Elsevier Scientific Publishing: Amsterdam, 1977.

(13) Unger, E.; Bobinger, U.; Dreybrodt, W.; Schweitzer-Stenner, R. *J. Phys. Chem.* **1993**, *97*, 9956.

(14) Jentzen, W. Ph.D. Thesis, University of Bremen, Germany, 1994.

(15) Karvounis, G.; Unger, E. Manuscript in preparation.

(16) Li, X.-Y.; Czernuszewicz, R. S.; Kincaid, J. R.; Stein, P.; Spiro, T. G. *J. Phys. Chem.* **1990**, *94*, 47.

(17) Shelnutt, J. A.; Cheung, L. D.; Chang; R. C. C.; Yu, N.-T.; Felton, R. H. *J. Chem. Phys.* **1977**, *66*, 3387.

(18) Bobinger, U.; Schweitzer-Stenner, R.; Dreybrodt, W. *J. Phys. Chem.* **1991**, *95*, 7625.

(19) (a) McClain, W. M. *J. Chem. Phys.* **1971**, *55*, 2789. (b) Verma A. L.; Bernstein, H. J. *J. Chem. Phys.* **1974**, *61*, 2560. (c) Zgierski, M. Z.; Pawlikowski, M. *J. Chem. Phys*. **1982**, *65*, 335.

(20) An earlier Raman study (ref 18) has reported that some of the high-frequency lines of Ni(OEP) in solution exhibit a dispersion of their depolarization ratios. This was interpreted in terms of symmetry-lowering distortion of the macrocycle from D_{4h} to S_4 symmetry. Unfortunately, the spectral slit widths used were not sufficient to decompose the strongly overlapping lines in their components. This is in particular severe because of the heterogeneity of the structure-sensitive lines. The present study, however, was carried out with much better spectral resolution and a more appropriate spectral analysis. We found no indication of a depolarization ratio dispersion. In accordance with the crystal data (ref 5a), this suggests that the effective molecular symmetry of the nonplanar conformer is probably at least D_{2d} rather than S_4.

(21) (a) Findsen, E. W.; Shelnutt, J. A.; Ondrias, M. R. *J. Phys. Chem.* **1988**, *92*, 307. (b) Crawford, B. A.; Ondrias, M. R.; Shelnutt, J. A. *J. Phys. Chem.* **1990**, *94*, 6647.

(22) (a) Bevington, P. R. In *Data reduction and error analysis for the physical science*; McGraw Hill: New York, 1969. (b) Gilch, H.; Dreybrodt, W.; Schweitzer-Stenner, R. *Biophys. J.* **1995**, *69*, 214.

(23) Alden, R. G.; Ondrias, M. R.; Shelnutt, J. A. *J. Am. Chem. Soc.* **1990**, *112*, 691.

(24) Jentzen, W.; Unger, E.; Turowska-Tyrk, I.; Song, X.; Nurco, D. J.; Medforth, C. J.; Smith, K. M.; Dreybrodt, W.; Schweitzer-Stenner, R.; W.; Scheidt, W. R.; Shelnutt, J. A. Manuscript in preparation.

(25) Cupane, A.; Leone, M.; Cordone, L.; Gilch, H.; Unger, E.; Dreybrodt, W.; Schweitzer-Stenner, R. *J. Phys. Chem.* **1996**, *100*, 14192−14197.

(26) Munro, O. Q.; Bradley, J. C.; Hancock, R. D.; Marques, H. M.; Marsicano, F.; Wade, P. W. *J. Am. Chem. Soc.* **1992**, *114*, 7218.

(27) Because all fundamental lines are assigned in the 1600-cm^{-1} region (ref 16) and the entire line ν_2 is of A_{1g}-type polarization, the additional underlying Raman line may result from a nonfundamental line with A_{1g} symmetry. For example, $2\nu_6$ (1608 cm^{-1}), $\nu_{25} + \nu_{23}$ (1609 cm^{-1}), and $\nu_{34} + \nu_{29}$ (1604 cm^{-1}) are possible candidates for overtone or combination lines. However, a significant intensity contribution to the Raman spectrum with B-band excitation by these nonfundamentals is unlikely because the fundamentals themselves are relatively weak. Moreover, the intensity of the overtone and combination lines in the 2600−3400-cm^{-1} region, resulting from strong fundamentals which are located between 1300 and 1700 cm^{-1}, are also weak when B-band excitation wavelengths are used. This implies that Fermi resonance interaction between the line ν_2 and a nonfundamental line must be considered to rationalize the intensity in the Raman spectra.

(28) Without regarding the spectral crowding in the ν_2 region, the line ν_2 can be decomposed consistently into two sublines at different excitation wavelengths and temperatures. At room temperature, the frequency position of the sublines are 1602 and 1608 cm^{-1}, and the corresponding widths are 13 cm^{-1} for the LF subline (pure Gaussian) and 11 cm^{-1} for the HF subline (pure Lorentzian). According to the decomposition at different temperatures, the intensity ratios of the sublines of ν_2 are significantly different from the intensity ratios of the sublines of ν_{19} and ν_{10}. Specifically, the slope in the van't Hoff plot is almost equal in magnitude but *opposite* in sign. Moreover, the different behavior of the sublines of ν_2 is further corroborated by their Raman excitation profiles. In contrast to the sublines of ν_{19} and ν_{10}, the maxima of the REPs of the HF and LF subline of ν_2 are similar. To sum up, these findings obviously indicate that the simple two-state model proposed in the text cannot explain *simultaneously* the REPs and temperature dependence of the sublines of ν_2, ν_{19}, and ν_{10}. But spectral crowding in the ν_2 region accounts for the disagreement between the line ν_2 and the lines ν_{19} and ν_{10}.

JP9533032